Journal of Zhejiang University-SCIENCE A (Applied Physics & Engineering)
ISSN 1673-565X (Print); ISSN 1862-1775 (Online)
www.jzus.zju.edu.cn; www.springerlink.com
E-mail: jzus@zju.edu.cn

Theoretical investigation into the effect of rail vibration dampers on the dynamical behaviour of a high-speed railway track*

Xin-biao XIAO, Ya-guang LI, Ting-sheng ZHONG, Xiao-zhen SHENG†‡

(*State Key Laboratory of Traction Power, Southwest Jiaotong University, Chengdu 610031, China*)

†E-mail: shengxiaozhen@hotmail.com

Received Oct. 22, 2016; Revision accepted May 10, 2017; Crosschecked July 7, 2017

Abstract: Installation of rail vibration dampers (rail dampers for short) onto rails between sleepers is one of the measures to control rail noise generation and roughness growth. Amid the rapid expansion of high-speed and underground railway networks in China, many suppliers are actively marketing and promoting their products, often giving confusing information. In this paper, a parametric study is used to investigate the effect of rail dampers on the dynamical behavior of a Chinese high-speed railway track. The Fourier transform-based method developed for analyzing dynamics of a railway track as an infinitely long periodic structure, with or without rail dampers, is applied in the investigation. It is hoped that results in this paper can help develop the understanding of the working mechanism of rail dampers, and provide useful information for product design and application.

Key words: Rail damper; Track dynamics; Dispersion curves; Vibration decay rate
http://dx.doi.org/10.1631/jzus.A1600697 **CLC number:** O324; U270

1 Introduction

Theoretical research and *in-situ* observations have shown that the pinned-pinned vibration of the rail, in which the fasteners behave like pins to the rail, plays an important role in noise radiation and roughness growth (Thompson, 2009). One of the measures for suppressing this pinned-pinned vibration is the use of rail vibration dampers (Maes and Sol, 2003; Thompson *et al.*, 2007; Croft *et al.*, 2009) which are installed on the rail between the sleepers. Rail dampers proposed by Thompson *et al.* (2007) and Croft *et al.* (2009) are frequency-tuned mass-spring systems (also often termed tuned mass damper, TMD), with either a single mass or two masses enclosed in an elastomeric material providing both stiffness and damping. The track model used by Thompson *et al.* (2007) is a simplified one in which the rail is represented as a Timoshenko beam on a continuous spring-mass-spring foundation representing the railpad, sleeper, and ballast, while Croft *et al.* (2009) considered the discrete supports to the rail. For a given wheel and wheel/rail roughness, a parameter study was presented by Thompson *et al.* (2007) on the effect of a rail damper on the sound power radiated from the track. In this parametric study, the mass and tuning frequency of the rail damper, and the train speed up to 160 km/h are varied. Wu (2008) investigated 'long' rail dampers and proposed certain design guidelines. When a damper is not short compared to the sleeper spacing, bending of the metal beam in the damper may play a role. However, it is demonstrated by Liu *et al.* (2009) that it is the rigid body motion of the beam of the damper that leads to the energy dissipation of rail vibration, whereas the bending deformation of the beam is a

‡ Corresponding author

* Project supported by the National Natural Science Foundation of China (Nos. U1434201 and 51475390), the Foundation of China Railway (No. 2015Z003-B), and the Scientific Research Foundation of State Key Laboratory of Traction Power (Nos. 2015TPL_T08 and 2017TPL_T01), China

ORCID: Xin-biao XIAO, http://orcid.org/0000-0001-5078-4817

minor factor. Therefore, a simple mass-spring model, instead of an advanced beam-spring model, is adequate to represent the rail damper. This observation also largely applies to other varieties of rail dampers appearing in the market.

While the studies (Thompson *et al*., 2007; Wu, 2008; Croft *et al.*, 2009; Liu *et al.*, 2009) all dealt with discretely distributed rail dampers, Thompson (2008) presented a study on a continuous damped vibration absorber to reduce broad-band wave propagation in a beam. The beam is either unsupported with the mass of the absorber connected to the beam via a layer of viscous springs, or supported via a viscous Winkler foundation under the damper mass. The value of this study lies in the simple formulae developed relating the absorber's behavior and its design parameters.

A railway track with fasteners/sleepers can be idealized as an infinitely long periodic structure. The period is equal to the sleeper spacing for a conventional ballasted track, or equal to the length of a slab if the track is a pre-cast slab track such as those used in China's high-speed railways. If identical rail dampers are installed on the rail at the same position (normally at mid-span) within each sleeper bay, then the track with the dampers is still an infinitely long periodic structure with the period unchanged. To evaluate the effect of rail dampers, calculations must be performed to predict various quantities for a track with or without rail dampers. These quantities include, for example, track responses to a harmonic load moving along the rail, dispersion curves of the periodic structure, vibration decay rates of the track in the track direction, wheel/rail interactions, and even wheel/rail rolling noise. Thus, different calculation methods have been developed in the past, including those based on the conventional finite element method (Thompson *et al*., 2007; Croft *et al.*, 2009), those based on the idea of 'mass on time-varying spring' (Nordborg, 2002; Wu, 2008; Liu *et al.*, 2009; Correa *et al.*, 2012), and those based on the Green function of the track (Mazilu, 2007; Mazilu *et al.*, 2011). Methods in the last two categories all make use of the periodicity of the track, so that a high computational efficiency and accuracy can be secured.

A Fourier transform-based method, firstly developed by the corresponding author of this paper for a conventional ballasted track (Sheng *et al.*, 2005), and then extended to a track with rail dampers (Sheng, 2015), can efficiently calculate track vibrations excited by a harmonic load of high frequency and moving at high speed. The main feature of the method is that the responses of the rail, sleepers, and dampers (if present) are all expressed in the form of a Fourier series, and each Fourier coefficient in the series is calculated as a Fourier transform from the wavenumber domain to the space (distance to the load) domain, both in the track direction. Based on Sheng *et al.* (2005) and Sheng (2015), the so-called time-domain moving Green function was then defined, derived, and discussed by Sheng and Xiao (2015) and Sheng *et al*. (2016b), and applied to deal with wheel/rail interactions by Sheng *et al.* (2016a). The effect of rail dampers of a particular design on the dynamics of a conventional ballasted track was also investigated by Sheng (2015) and Sheng *et al.* (2016b). The damper is tuned to 1000 Hz, close to the pinned-pinned frequency of the original track.

The track type of most of the high-speed railways in China is a non-ballasted and pre-cast slab track. To protect the slabs, the rail fastening systems are soft, potentially leading to a number of issues (Jin, 2014; Han *et al*., 2015) and providing market opportunities in the high-speed railway sector for rail damper suppliers. Rail dampers of various designs, some of which are tuned to frequencies much lower than the pinned-pinned frequency of the track, are being recommended to high-speed railway operators.

In order to give useful information for the design and application of rail dampers, and to further develop the understanding of the mechanisms involved, a parametric study is carried out in this paper to investigate the effect of rail damper parameters on the vibrational behavior of a Chinese high-speed railway track. Methods developed by Sheng *et al*. (2005) and Sheng (2015) for analyzing the dynamics of a rail track as an infinitely long periodic structure, with or without rail dampers, are applied in the parametric study. In this study, the track and rail dampers are described first. Then, a rewriting in a simpler form of the main equations derived by Sheng (2015) is shown. At last, results of the parametric study are presented.

Note that only vertical track dynamics is considered in this study, since in general this is the main mechanism of track noise generation.

2 Dynamical modelling of the high-speed railway track and rail damper

2.1 Description of the track

The track considered in this study is the Chinese CRTS II slab track, consisting of rails, rail fastener systems, pre-stressed concrete slabs with cast-in sleepers, a layer of concrete-asphalt (CA) mortar, and a concrete base (Fig. 1). As can be seen in Fig. 1, to model a fastener, two springs are inserted between the rail and slab, one being a vertical spring providing vertical stiffness to the rail and slab, and the other being a rotational spring providing rotational stiffness. These two springs are positioned at the same point. The parameters of the track are listed in Table 1 which are taken from Zhai *et al.* (2015) and also partially checked through receptance measurement. It can be seen that the stiffness of the railpad is very low, only 2.5×10^7 N/m, and the slab and the CA layer are of much higher rigidity. Thus, rail vibration will not be significantly affected by vibration of the slabs. Since the focus of this study is the effect of rail dampers on the vertical vibration of the rail, the track model may be simplified to a Timoshenko beam supported at regular positions by spring pairs representing the fastener systems (Fig. 2, where $\mathrm{i}=(-1)^{0.5}$). A spring pair provides both translational (in the vertical direction) and rotational (in the xz-plane) stiffness for the rail. If the vertical stiffness of the railpad is denoted by k_P, then the rotational stiffness is given by $b_\mathrm{s}^2k_\mathrm{p}/12$, where b_s is the longitudinal length of the railpad. The sleeper spacing L=0.65 m.

A vertical harmonic load of radian frequency Ω is moving at speed c along the rail, and the amplitude of the load is denoted by P_0. At t=0, the load is at x_0 which is measured from the 0th fastener. It can be seen from Fig. 2 that the fasteners are numbered in such a way that the x-coordinate of the jth fastener is jL, where $j=-\infty, \cdots, -1, 0, 1, \cdots, \infty$. The bay between the jth fastener and the $(j+1)$th fastener is termed the jth bay.

Fig. 3 shows the rail with rail dampers. Two rail dampers are installed either side of the rail at the mid-span of each sleeper bay. The mass of a rail damper is allowed to vibrate vertically and rotationally in the xz-plane. For clarity, in what follows, the two rail dampers in a sleeper bay are collectively treated as a single rail damper. As can be seen from Fig. 3, rail dampers are also numbered, and the x-coordinate of the jth damper is $0.5L+jL$, where $j=-\infty, \cdots, -1, 0, 1, \cdots, \infty$.

Table 1 Parameters for the vertical dynamics of the track

Parameter	Value
Density of the rail, ρ (kg/m^3)	7850
Young's modulus of the rail, E (N/m^2)	2.1×10^{11}
Shear modulus of the rail, G (N/m^2)	0.81×10^{11}
Cross-sectional area of the rail, A (m^2)	7.69×10^{-3}
Second moment of area of the rail, I (m^4)	30.55×10^{-6}
Shear coefficient of the rail cross-section, κ	0.4
Vertical railpad stiffness, k_P (N/m)	2.5×10^7
Railpad loss factor, η_P	0.25
Sleeper spacing, L (m)	0.65
Length of the slab, L_S (m)	6.45
Width of the slab, b_S (m)	2.55
Thickness of the slab, h_S (m)	0.2
Young's modulus of the slab, E_S (N/m^2)	3.45×10^{10}
Poisson's ratio of the slab, v_S	0.2
Density of the slab, ρ_S (kg/m^3)	2500
Vertical stiffness of CA layer per unit area, k_C (N/m^3)	6.67×10^9

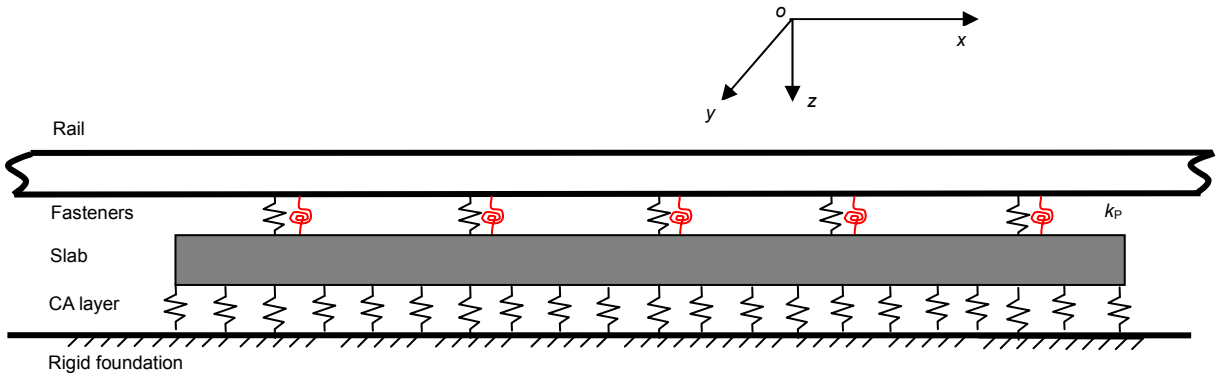

Fig. 1 A sketch of the slab high-speed railway track

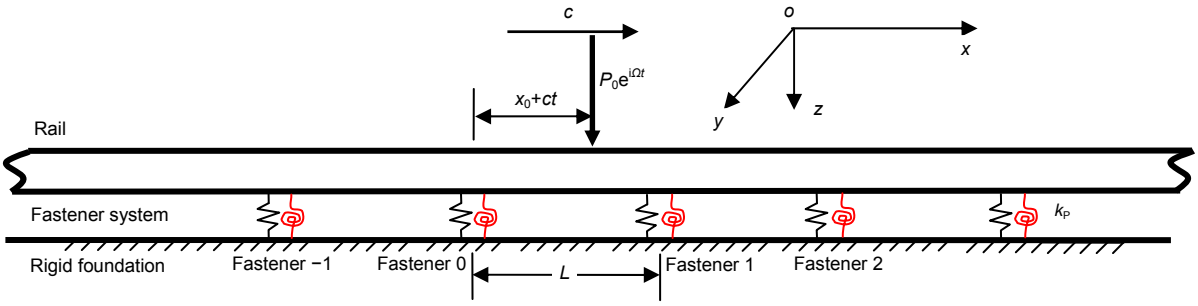

Fig. 2 Model of the track without rail dampers

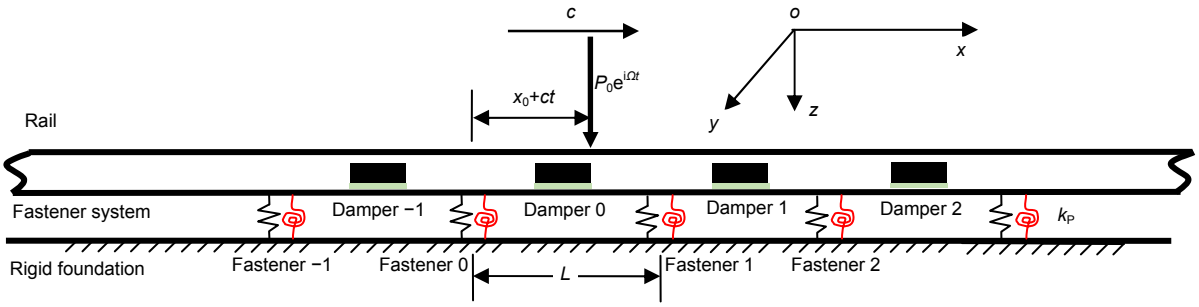

Fig. 3 Model of the track with rail dampers

2.2 Differential equations of motion of the track with rail dampers

According to Timoshenko beam theory, the differential equation for the rail is given by

$$\begin{aligned}&\rho A\frac{\partial^2 w}{\partial t^2}-\kappa AG\frac{\partial^2 w}{\partial x^2}+\kappa AG\frac{\partial \psi}{\partial x}\\&\quad=P_0\delta(x-x_0-ct)\mathrm{e}^{\mathrm{i}\Omega t}\\&\qquad+\sum_{j=-\infty}^{\infty}\sum_{s=1}^{S}\delta(x-x_s-jL)F_{js}(t),\end{aligned}\tag{1}$$

$$\begin{aligned}&\rho I\frac{\partial^2 \psi}{\partial t^2}-EI\frac{\partial^2 \psi}{\partial x^2}-\kappa AG\frac{\partial w}{\partial x}+\kappa AG\psi\\&\quad=\sum_{j=-\infty}^{\infty}\sum_{s=1}^{S}\delta(x-x_s-jL)M_{js}(t),\end{aligned}\tag{2}$$

where w is the vertical displacement (directed downwards) of the rail and ψ is the rotation angle (directed clockwise) of the cross-section due to the bending moment only; $F_{j1}(t)$ is the vertical force applied to the rail by the jth fastener and $F_{j2}(t)$ the force applied by the damper in the jth sleeper bay; $M_{j1}(t)$ is the torque exerted on the rail in the longitudinally vertical plane by the jth fastener and $M_{j2}(t)$ the torque from the damper in the jth sleeper bay; finally, S=2, x_1=0 (the x-coordinate of the 0th fastener), and x_2=L/2 (the x-coordinate of the 0th rail damper). Eqs. (1) and (2) may be written as

$$\begin{aligned}&\boldsymbol{M}\ddot{\boldsymbol{q}}(x,t)+\boldsymbol{K}_0\boldsymbol{q}(x,t)\\&\qquad+\boldsymbol{K}_1\frac{\partial}{\partial x}\boldsymbol{q}(x,t)-\boldsymbol{K}_2\frac{\partial^2}{\partial x^2}\boldsymbol{q}(x,t)\\&\quad=\boldsymbol{p}_0\mathrm{e}^{\mathrm{i}\Omega t}\delta(x-x_0-ct)\\&\qquad+\sum_{j=-\infty}^{\infty}\sum_{s=1}^{S}\delta(x-x_s-jL)\boldsymbol{f}_{js}(t),\end{aligned}\tag{3}$$

where

$$\boldsymbol{q}=\begin{Bmatrix}w\\ \psi\end{Bmatrix},\ \boldsymbol{M}=\begin{bmatrix}\rho A & 0\\ 0 & \rho I\end{bmatrix},\ \boldsymbol{K}_0=\begin{bmatrix}0 & 0\\ 0 & \kappa AG\end{bmatrix},$$
$$\boldsymbol{K}_1=\begin{bmatrix}0 & \kappa AG\\ -\kappa AG & 0\end{bmatrix},\ \boldsymbol{K}_2=\begin{bmatrix}\kappa AG & 0\\ 0 & EI\end{bmatrix},\tag{4}$$

$$\boldsymbol{p}_0=\begin{Bmatrix}1\\ 0\end{Bmatrix},\ \boldsymbol{f}_{js}(x,t)=\begin{Bmatrix}F_{js}(t)\\ M_{js}(t)\end{Bmatrix}.\tag{5}$$

2.3 Receptance matrices of fasteners and rail dampers

The receptance matrix of a fastener (a rail damper) associated with the degrees of freedom

(DOFs), denoted by w and ψ, of the rail is used to describe the dynamics of the fastener (the rail damper). An element, $H_{ij}(\omega)$, of the receptance matrix, is the displacement in the ith DOF due to a unit harmonic force (or torque) of frequency ω applied in the jth DOF (Fig. 4).

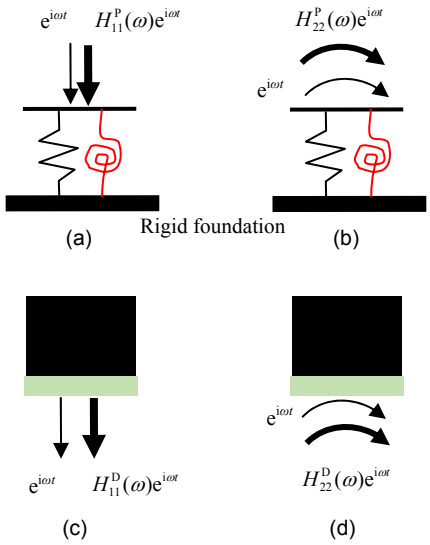

Fig. 4 Definitions of receptances for a fastener and a rail damper: (a) vertical receptance of the fastener; (b) rotational receptance of the fastener; (c) vertical receptance of the rail damper; (d) rotational receptance of the rail damper (thin arrows stand for force or moment and thick arrows for responses)

Thus, the receptance matrix of a fastener is given by

$$\boldsymbol{H}_1(\omega)=\begin{bmatrix} H_{11}^{P}(\omega) & 0 \\ 0 & H_{22}^{P}(\omega)\end{bmatrix}=\begin{bmatrix} \dfrac{1}{k_P} & 0 \\ 0 & \dfrac{12}{b_S^2 k_P}\end{bmatrix}, \tag{6}$$

and the receptance matrix of the damper in a sleeper bay is given by

$$\begin{aligned}\boldsymbol{H}_2(\omega) &= \begin{bmatrix} H_{11}^{D}(\omega) & 0 \\ 0 & H_{22}^{D}(\omega)\end{bmatrix} \\ &= \begin{bmatrix} -\dfrac{k_{Dw}-m_D\omega^2}{m_D k_{Dw}\omega^2} & 0 \\ 0 & -\dfrac{k_{D\psi}-J_D\omega^2}{J_D k_{D\psi}\omega^2}\end{bmatrix},\end{aligned} \tag{7}$$

where m_D is the mass of the damper, J_D is the inertia moment of the damper, k_{Dw} is the vertical stiffness of the damper spring, and $k_{D\psi}$ is the rotational stiffness of the damper spring. The loss factors of the dampers are denoted by η_D. Eq. (7) shows that, at the tuned frequency of the damper, that is $\omega_D=(k_{Dw}/m_D)^{1/2}$, the receptance reaches a minimum and the constraint provided by the damper to the rail reaches a maximum.

3 Solutions to equations governing responses of the rail and dampers

Equations giving the responses of the rail and dampers are listed in this section. They are simplified from corresponding equations derived by Sheng (2015).

The response of the rail is given by

$$\begin{aligned}\boldsymbol{q}(x',t)=&\left[\frac{\boldsymbol{p}_0 e^{i\Omega t}}{2\pi}\int_{-\infty}^{\infty}[\boldsymbol{D}(\beta,\omega)]^{-1}e^{i\beta x'}d\beta\right.\\ &\left.+\sum_{j=-\infty}^{\infty}\left(-\frac{\boldsymbol{p}_0 e^{i\Omega t}}{2\pi L}e^{-i2\pi j(x'+x_0+ct)/L}\boldsymbol{R}(\beta_j,\omega)\right)\right],\end{aligned} \tag{8}$$

$$\begin{aligned}\boldsymbol{R}(\beta_j,\omega)=&\int_{-\infty}^{\infty}[\boldsymbol{D}(\beta_j,\omega)]^{-1}\boldsymbol{C}(\beta_j)\\ &\times[\boldsymbol{A}(\beta)]^{-1}\boldsymbol{B}(\beta)[\boldsymbol{D}(\beta,\omega)]^{-1}e^{i\beta x'}d\beta,\end{aligned}$$

where $x'=x-x_0-ct$ is the coordinate of the observation point of the rail relative to the moving load, β is the wavenumber, $\boldsymbol{A}$ is a matrix of order $2S\times 2S$ (here $S=2$), $\boldsymbol{B}$ is a matrix of order $2S\times 2$, $\boldsymbol{C}$ is a matrix of order $2\times 2S$, and $\boldsymbol{D}$ is a matrix of order 2×2. By defining

$$\boldsymbol{U}=\begin{bmatrix}1 & 0\\ 0 & 1\end{bmatrix}, \tag{9}$$

$$\omega=\Omega-\beta c, \tag{10}$$

then

$$\boldsymbol{D}(\beta,\omega)=-\omega^2\boldsymbol{M}+\boldsymbol{K}_0+i\beta\boldsymbol{K}_1+\beta^2\boldsymbol{K}_2, \tag{11}$$

$$\beta_j=\beta-\frac{2\pi j}{L}, \tag{12}$$

$$\boldsymbol{C}(\beta_j)=\left(e^{-i\beta_j x_1}\boldsymbol{U},e^{-i\beta_j x_2}\boldsymbol{U},\cdots,e^{-i\beta_j x_S}\boldsymbol{U}\right), \tag{13}$$

$$\boldsymbol{B}(\beta)=\left(e^{i\beta x_1}\boldsymbol{U},e^{i\beta x_2}\boldsymbol{U},\cdots,e^{i\beta x_S}\boldsymbol{U}\right)^{T}, \tag{14}$$

where the superscript T denotes matrix transpose.

$$\boldsymbol{A}(\beta)=([\boldsymbol{A}(\beta)]_{rs})_{r,\,s=1,\,2,\,\cdots,\,S}, \tag{15}$$

$$[\boldsymbol{A}(\beta)]_{rs}=\left(\frac{1}{L}\sum_{j=-\infty}^{\infty}[\boldsymbol{D}(\beta_j,\omega)]^{-1}\mathrm{e}^{\mathrm{i}\beta_j(x_r-x_s)}\right)+\delta_{rs}\boldsymbol{H}_r(\omega), \tag{16}$$

where δ_{rs} is the Kronecker delta.

By defining

$$\boldsymbol{G}(\omega)=\begin{bmatrix}0 & 0 & \dfrac{1}{-m_{\mathrm{D}}\omega^2} & 0\end{bmatrix}, \tag{17}$$

the vertical displacement of the mass of the rail damper in the jth sleeper bay is given by

$$g_j(t)=\frac{1}{2\pi}\boldsymbol{p}_0\mathrm{e}^{\mathrm{i}\Omega t}\times\left(\int_{-\infty}^{\infty}\boldsymbol{G}(\omega)[\boldsymbol{A}(\beta)]^{-1}\boldsymbol{B}(\beta)[\boldsymbol{D}(\beta,\omega)]^{-1}\mathrm{e}^{\mathrm{i}\beta(jL-x_0-ct)}\mathrm{d}\beta\right). \tag{18}$$

Damping is introduced to the above equations by using complex stiffness. For example, the stiffness of the railpad is replaced with $k_{\mathrm{p}}(1+i\eta_{\mathrm{P}}\,\mathrm{sgn}(\omega))$, where η_{P} is the railpad loss factor, ω is given in Eq. (10), and sgn is the sign function.

4 Parametric study

To limit the number of cases to be studied, the parametric study for the rail dampers is first performed for two parameters: damper loss factor and tuned frequency. Each parameter has a low, a medium, and a high level. For the damper loss factor, these levels are 0.15, 0.35, and 0.55, and for the tuned frequency, they are 250, 500, and 1000 Hz.

Cases to be calculated and associated parameters are listed in Table 2, including Case 0 in which there is no rail damper present (i.e., the original track). It should be noted that, a damper has two vibrational modes and natural frequencies, one related to translational vibration in the vertical direction and the other related to rotational vibration in the xz-plane. In all the cases, these two natural frequencies have fixed proportionality which is determined based on a market-available damper design. Parameters for the rotational vibration of the damper inertia are also listed in Table 2 but bracketed.

It can be seen from Table 2 that the natural frequency of the dampers is tuned by changing the stiffness. For a given tuned frequency, the effect of the damper mass will also be investigated, which is presented in the end of this section.

For each of the cases in Table 2, results are produced for: (1) dispersion curves (Section 4.1); (2) bounding frequencies calculated from single bays (Section 4.2); (3) responses of the rail and a damper due to a unit stationary harmonic load applied at the rail just above the rail damper (Section 4.3); (4) vibration decay rates of the rail due to the above harmonic load (Section 4.4); (5) vibration decay rate of the rail due to a unit harmonic load moving at 300 km/h (83 m/s) along the rail (Section 4.5); (6) vibration energy level of the track due to the above moving load (Section 4.6).

It can be seen that the parametric study is performed not only for a moving load but also for a stationary load. This is because the rail vibration decay rate is normally measured for a stationary load which is applied at a fixed point of the rail using an instrumented hammer.

4.1 Dispersion curves

Dispersion curves are used to describe the free wave characteristics of a track as an infinitely long periodic structure. For a given frequency ω, the real wavenumbers satisfying $\det(\boldsymbol{A}(\beta,\omega))=0$ are the characteristic propagating wavenumbers of the track at that frequency, where matrix $\boldsymbol{A}(\beta,\omega)$ is given by Eqs. (15) and (16). It is shown by Sheng *et al.* (2005) that, if β is a propagating wavenumber, then $\overline{\beta}+2\pi j/L$ is as well, where j is any integer. Therefore, for a given frequency range, either there are an infinite number of propagating wavenumbers, or there are none. In case of the former, the frequency range is called a pass band; it is a stop band if the latter is true. Stop bands and pass bands appear alternately. Existence of stop bands is beneficial for controlling noise radiation from the rail (Thompson *et al.*, 2007; Thompson, 2009). This is because, if excited frequencies are within a stop band, dominant

Table 2 Rail damper parameters for the parametric study (the values are for two dampers in a sleeper bay)

Case	Mass (kg) (inertia moment (kg·m^2))	Tuned frequency (Hz)	Vertical stiffness (N/m) (rotational stiffness (N·m))	Loss factor
0	0	–	–	–
1	15 (0.058)	250 (232)	0.37×10^8 (0.12×10^6)	0.15
2	15 (0.058)	500 (464)	1.48×10^8 (0.49×10^6)	0.15
3	15 (0.058)	1000 (928)	5.92×10^8 (1.97×10^6)	0.15
4	15 (0.058)	250 (232)	0.37×10^8 (0.12×10^6)	0.35
5	15 (0.058)	500 (464)	1.48×10^8 (0.49×10^6)	0.35
6	15 (0.058)	1000 (928)	5.92×10^8 (1.97×10^6)	0.35
7	15 (0.058)	250 (232)	0.37×10^8 (0.12×10^6)	0.55
8	15 (0.058)	500 (464)	1.48×10^8 (0.49×10^6)	0.55
9	15 (0.058)	1000 (928)	5.92×10^8 (1.97×10^6)	0.55

characteristic waves of the track which are excited are evanescent ones, thus limiting to a great extent the length of the rail effective for sound radiation.

Propagating wavenumbers plotted against frequencies are termed dispersion curves of the track. Such curves may be produced by generating a contour plot of $20\lg[1/|\det(\boldsymbol{A}(\beta,\omega))|]$ on the frequency-wavenumber plane for a stationary load (i.e., c=0), as shown in Figs. 5–8. In Figs. 5–8, dispersion curves are bright curves. A point on a dispersion curve defines a wavenumber and a frequency. If there is no damping in the track, the periodically supported rail allows free vibration at that frequency to propagate along the rail without attenuation.

Bounding frequencies separating a pass band and a stop band are indicated in Figs. 5–8 using arrows. The minimum (in magnitude) wavenumbers at these frequencies are either equal to 0, or equal to $\pi/L=\pi/0.65=4.833$ (rad/m) (Sheng *et al.*, 2005).

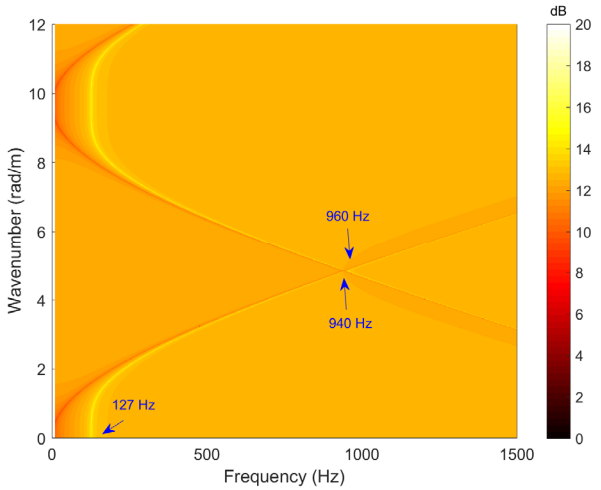

Fig. 5 Dispersion curves of the original track. There are three bounding frequencies: 127 Hz (II, S), 940 Hz (I, S), and 960 Hz (II, A)

In the captions of Figs. 5–8, there are two letters bracketed after each frequency. Letters I and II mean the frequency is a modal frequency of type I and type II, respectively, in a single bay of the track, and letters S and A mean that the associated modal shape is symmetric and anti-symmetric, respectively. For more details, see Section 4.2.

Fig. 5 shows the dispersion curves of the original track. The frequency band up to 127 Hz is the first stop band. The frequency of 127 Hz is the resonance frequency of the rail on the stiffness of the fasteners. The band between 940 Hz and 960 Hz is also a stop band. Due to the low stiffness of the railpads, the width of this stop band is rather narrow, only about 20 Hz. The frequency of 940 Hz is the pinned-pinned (the fasteners behave like pins with rotational stiffness to the rail) frequency. The free vibration wave at 960 Hz is a mode in which the rail has maximum vertical displacement at a fastener but zero vertical displacement at mid-span. In the frequency range up to 1500 Hz, the total width of the stop bands is only 147 Hz, making the track potentially noisy.

Fig. 6 shows the dispersion curves of the track with rail dampers tuned to 250 Hz (in what follows, the frequency mentioned in the phrase ‘dampers tuned to a frequency’ is the natural frequency of the dampers in vertical vibration, and the natural frequency for rotational vibration is also tuned accordingly since the ratio between the vertical and rotational natural frequencies is fixed). The band up to 104 Hz is the first stop band. The frequency of 104 Hz

is the resonance frequency of the rail and dampers on the stiffness of the railpads. A new stop band from 244 Hz to 300 Hz is created by the dampers. The stop band between 940 Hz and 960 Hz of the original track is slightly altered by the dampers. In the frequency range of 0 to 1500 Hz, the total width of the stop bands is 180 Hz.

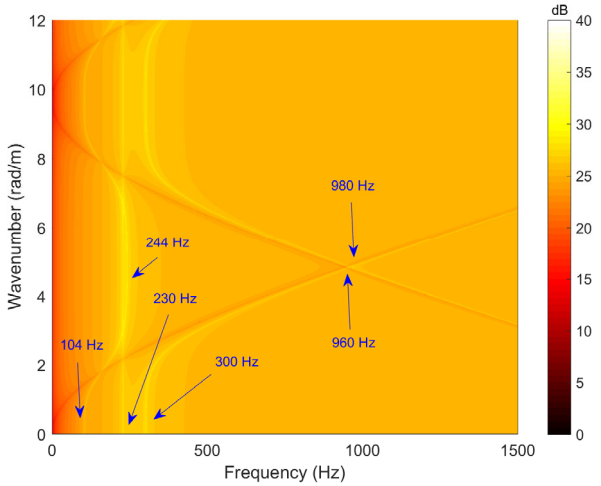

Fig. 6 Dispersion curves of the track with dampers tuned to 250 Hz. Bounding frequencies are 104 Hz (I, S), 244 Hz (II, S), 300 Hz (I, S), 960 Hz (I, A), and 980 Hz (II, S)

Fig. 7 shows the dispersion curves of the track with rail dampers tuned to 500 Hz. The first stop band contains frequencies up to 106 Hz. Two new stop bands are created by the rail dampers, one being from 440 Hz to 460 Hz, and the other being from 460 Hz to 580 Hz. The stop band between 940 Hz and 960 Hz of the original track is evidently altered by the dampers, becoming a wider stop band from 964 Hz to 1060 Hz. In the frequency range of 0 to 1500 Hz, the total width of the stop bands is 342 Hz.

Fig. 8 shows the dispersion curves of the track with rail dampers tuned to 1000 Hz, a little higher than the pinned-pinned frequency of the original track (940 Hz). The first stop band is up to 108 Hz. Two new stop bands are created by the rail dampers, one being from 625 Hz to 860 Hz, and the other being from 914 Hz to 1016 Hz. The stop band between 940 Hz and 960 Hz of the original track is significantly altered by the dampers, becoming much wider, 1084 Hz to 1448 Hz. In the frequency range of 0 to 1500 Hz, the total width of the stop bands is 809 Hz.

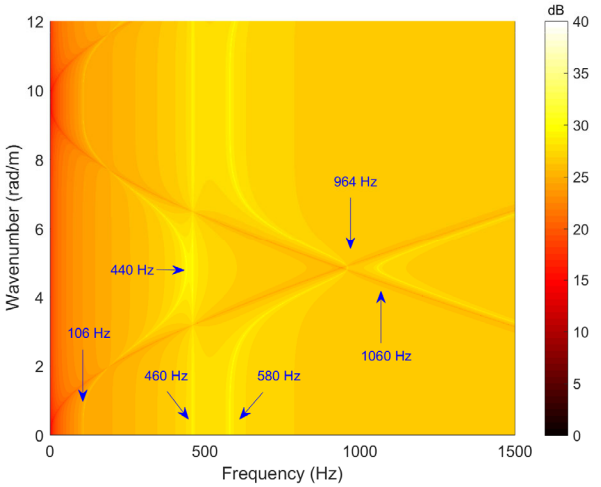

Fig. 7 Dispersion curves of the track with dampers tuned to 500 Hz. Bounding frequencies are 106 Hz (I, S), 440 Hz (II, S), 460 Hz (I, A; II, A), 580 Hz (I, S), 964 Hz (I, A), and 1060 Hz (II, S)

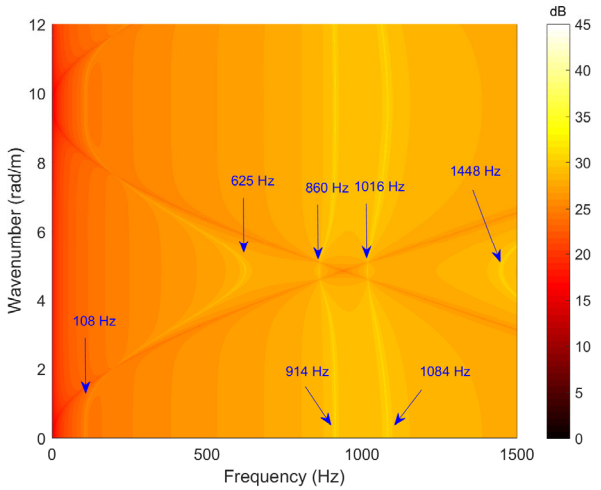

Fig. 8 Dispersion curves of the track with dampers tuned to 1000 Hz. Bounding frequencies are 108 Hz (I, S), 625 Hz (II, S), 860 Hz (I, A), 914 Hz (II, A), 1016 Hz (I, A), 1084 Hz (I, S), and 1448 Hz (II, S)

From the above it can be seen that, rail dampers not only increase the band width of the stop band associating with the pinned-pinned frequency of the original track, but also create new stop bands. In terms of the total width of stop bands, the damper of a given mass should be tuned to a frequency close to the pinned-pinned frequency of the original track. More quantitatively, the total width of stop bands is 180 Hz for dampers tuned to 250 Hz, compared with 809 Hz when the dampers are tuned to 1000 Hz.

Note that, for sound radiation from the rail, the width of pass or stop bands is not the whole story. Pass or stop bands are mainly a phenomenon of undamped systems. For a damped system the wave decay outside the stop bands is also very important. In other words, dampers of good design should not only increase the width of stop bands, but for pass bands, also create a vibration wave decay rate which is higher than that of the original track. Vibration decay rate will be discussed in Sections 4.4 and 4.5.

4.2 Determination of bounding frequencies based on a single bay of the track

It is explained by Sheng and Li (2007), following the principle described by Mead (1996), that the bounding frequencies identified above are natural frequencies of a single bay of the track with proper boundary conditions. The boundary conditions are such either that the two ends of the rail are allowed to slide in the vertical direction only (termed type I single bay), or that the two ends of the rail are hinged (termed type II single bay). These two types of single bay are depicted in Table 3.

For each of the single bays, modal analysis is performed using the finite element method, and the calculated modal frequencies are listed in Table 3 with a letter S or A, and a number 0 or π/L. Since the single bays are symmetric structures, their modal shapes are either symmetric (S) or anti-symmetric (A). For both the single bays, the rails at mid-span and the damper have zero vertical displacement in an anti-symmetric mode. The results of modal analysis of single bays can be used to explain resonances or anti-resonances at the bounding frequencies, see Section 4.3.

As can be seen in Figs. 5–8, the wavenumber corresponding to a bounding frequency is either 0 or π/L. If a bounding frequency is the natural frequency of an S mode (A mode) of type I (type II) single bay, then the corresponding wavenumber is 0. If a bounding frequency is the natural frequency of an A mode (S mode) of type I (type II) single bay, then the corresponding wavenumber is π/L.

Table 3 shows that, compared to the original track, installation of rail dampers creates new modal frequencies for the single bays. A result of this is to increase the bandwidth of stop bands for the track as an infinitely long periodic structure.

4.3 Responses of the track due to a stationary harmonic load

For a stationary unit harmonic load applied at the rail above a rail damper, the responses of the rail and dampers can be calculated by letting c=0 and x_0=L/2 in the equations listed in Section 3. It can be seen that the integrals appearing in these equations are all in the form of inverse Fourier transforms from β (wavenumber) domain to x' (position relative to the load) domain. To produce results for a large number of dampers and for a large number of points along the rail, the inverse fast Fourier transform (FFT) technique is used to perform the integrations. Inverse

Table 3 Two types of single bay and associated natural frequencies in Hz

Original track	Damper of 250 Hz	Damper of 500 Hz	Damper of 1000 Hz	Original track	Damper of 250 Hz	Damper of 500 Hz	Damper of 1000 Hz
127 (S, 0)	104 (S, 0)	106 (S, 0)	108 (S, 0)	940 (S, π/L)	230 (A, 0)	440 (S, π/L)	625 (S, π/L)
960 (A, π/L)	230 (A, π/L)	460 (A, π/L)	860 (A, π/L)	–	244 (S, π/L)	460 (A, 0)	914 (A, 0)
–	300 (S, 0)	580 (S, 0)	1016 (A, π/L)	–	980 (S, π/L)	1060 (S, π/L)	1448 (S, π/L)
–	960 (A, π/L)	964 (A, π/L)	1084 (S, 0)	–	–	–	–

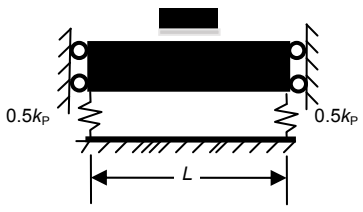

Type I single bay

Type II single bay

FFTs are performed on an array of 3200 wavenumbers ranging from −25.12 rad/m to 25.12 rad/m at spacing $\Delta\beta=2\pi\times0.0025$ rad/m. According to the principle of FFT, responses are available between $x'=-200$ m and 200 m at spacing $\Delta x'=0.125$ m. They can then be used to work out vibration decay rates for the rail and dampers, as presented in Sections 4.4 and 4.5.

It has been explained by Mead (1996) and Sheng and Li (2007) that, peaks appear in the receptance of the rail at or around (due to damping) some bounding frequencies of the track as a periodic structure, indicating the excitation of the associated modes of the single bays. Since the force is applied at mid-span, only symmetric modes of the single bays are possibly excited. This is illustrated in Fig. 9. This figure shows the displacement amplitude of the rail at the loading point due to a unit stationary harmonic load applied at mid-span. The solid curve is for the original track, the dashed curve is for the track with dampers tuned to 250 Hz (tuned frequency, TF), and the dash-dotted curve is for the displacement of the damper just under the load. Damper loss factor (DLF) is set to be 0.15.

It can be seen from Fig. 9 that, for the original track, only two peaks appear in the response of the rail for the frequency range shown. One is at 127 Hz, the first bounding frequency (Fig. 5), and the other is at 940 Hz, the pinned-pinned frequency where the fasteners behave like pins and the mid-span has the maximum response of all the positions.

For the track with dampers tuned to 250 Hz, peaks appear in the response of the rail at 104 Hz and 316 Hz, and dips appear at 252 Hz and 960 Hz. In the mode at 104 Hz, the rail and all the dampers vibrate in phase, making the response of the damper also show a peak at the same frequency. Around 252 Hz, there is a dip for the rail but a broad peak for the damper. This is because the dampers behave like dynamic vibration absorbers to the rail. For both the rail and damper, there is a dip at 960 Hz. From Table 3 it is seen that this frequency is the natural frequency of an A mode of type I single bay. Thus, this is also a 'pinned-pinned' frequency of the rail, but this time, the dampers, rather than the fasteners, behave like pins to the rail.

Figs. 10 and 11 provide comparisons in displacement of the rail at the loading point between the original track and the track with dampers tuned to 500 Hz (Fig. 10) and 1000 Hz (Fig. 11). The displacement of the damper just under the load is also displayed. The damper loss factor is 0.35.

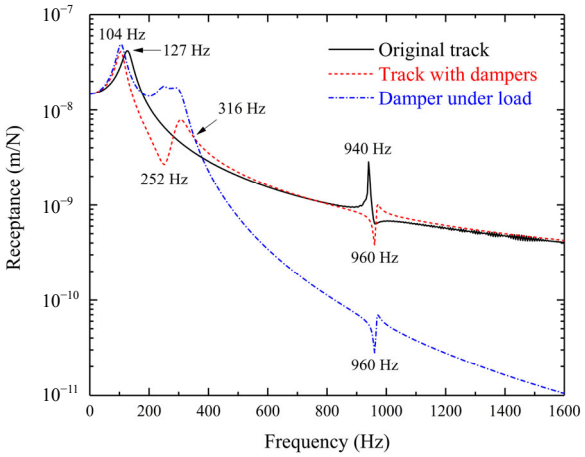

Fig. 9 Displacement of the rail (TF 250 Hz, DLF 0.15)

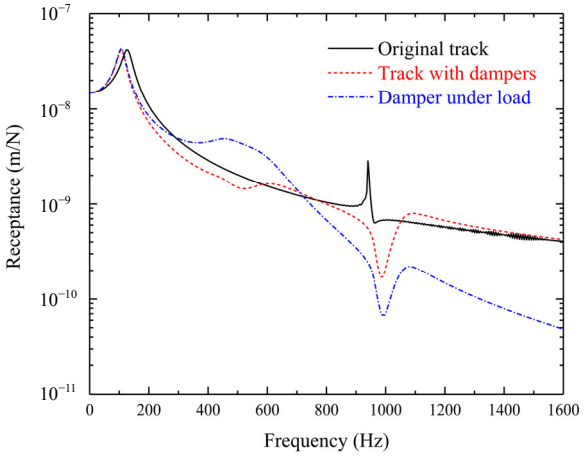

Fig. 10 Displacement of the rail (TF 500 Hz, DLF 0.35)

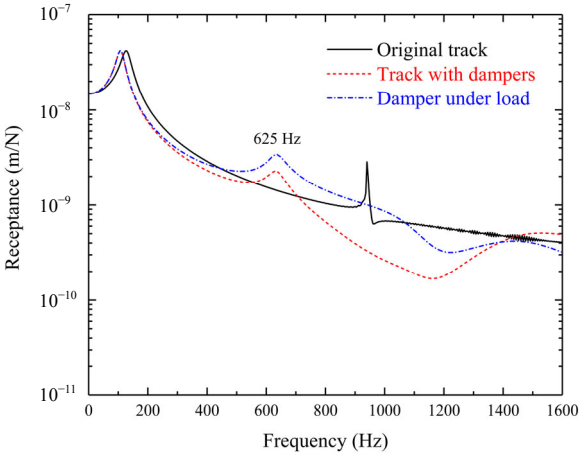

Fig. 11 Displacement of the rail (TF 1000 Hz, DLF 0.35)

Firstly, it can be seen from Figs. 9–11 that for frequencies lower than a certain value, the damper vibrates more strongly than the rail, and this value increases with the tuned frequency of the dampers. For those frequencies, noise radiated from the dampers may be not insignificant if compared to that from the rail.

Secondly, both Figs. 9 and 10 indicate that the dampers, rather than the fasteners, behave like pins to the rail at a frequency just below 1000 Hz. The explanation could be that around this frequency, the dynamic stiffness provided by the damper is higher than that of the fastener. However, when the damper is tuned to 1000 Hz, both the response of the rail and that of the damper have a peak at 625 Hz, as shown in Fig. 11. From Table 3 it is seen that this frequency is the natural frequency of an S mode of type II single bay, indicating that it is a pinned-pinned frequency with the fasteners behaving like pins to the rail. That this frequency (625 Hz) is much lower than the original pinned-pinned frequency (940 Hz) is due to the fact that the mass of the damper also takes part in this pinned-pinned vibration.

4.4 Vibration decay rates of the rail for a stationary harmonic load

For a stationary harmonic load applied at the rail above a damper, the track exhibits a vibration pattern which is symmetric about the load, and the vibration decays along the track at the same rate either sides of the load. The rate of vibration decaying along the rail may be worked out by plotting the vibration level against distance from the load, as shown in the upper plot of Fig. 12 for the rail of the original track at 400 Hz. Vibration level is defined as $20\lg(|w(x, 0)|)$. Two straight lines can be seen. The slope in magnitude of any one straight line is the decay rate, in dB/m, of vibration waves along the rail. It is also noticed that there is a small area in the vicinity of the load over which the decay rate is much higher. This is because in the vicinity of the load the near field wave and propagating wave usually have equal amplitudes so the vibration level drops quickly by around 3 dB due to the high decay of the near field wave.

To be consistent, in what follows, the vibration decay rate of the rail is calculated to be the difference between the vibration level of the rail at the 4th (j=4) fastener (2.275 m from the load) and that at the 21th (j=21) fastener (13.325 m from the load), divided by the distance between these two dampers (11.05 m).

The vibration decay rate of the rail of the original track is presented in the lower plot of Fig. 12 as a function of load frequency. It can be seen that, the decay rate is rather low, less than 0.5 dB/m, except for frequencies within the first stop band, that is, below the first bounding frequency of 127 Hz.

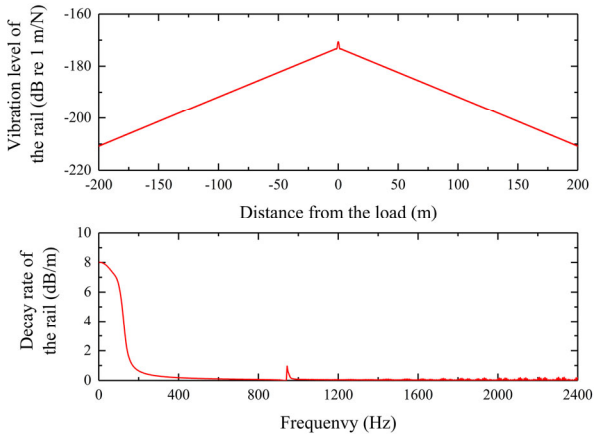

Fig. 12 Vibration characteristics of the original track

Fig. 13 shows the vibration decay rates of the rail with dampers tuned to 250 Hz (thin lines), 500 Hz (thicker lines), and 1000 Hz (the thickest lines), and for the three values of damper loss factor: 0.15 (solid line), 0.35 (dashed line), and 0.55 (dash-dotted line).

It can be seen that, in the first stop band, the decay rate is almost identical to that of the original track. However, in a frequency band around the tuned frequency of the dampers, the decay rate of the rail is significantly increased. This frequency band roughly corresponds to the stop band approximately centered at the tuned frequency of the dampers (244–300 Hz for dampers tuned to 250 Hz; 460–580 Hz for dampers tuned to 500 Hz; 625–1448 Hz for dampers tuned to 1000 Hz). For frequencies sufficiently higher than the tuned frequency, a higher loss factor results in a higher decay rate; for frequencies at and near the tuned frequency, a higher loss factor does not necessarily mean a higher decay rate.

Figs. 12 and 13 also show that, in the stop band (940–960 Hz in Fig. 6, 960–980 Hz in Fig. 7, and 964–1060 Hz in Fig. 8), the decay rate of the rail without dampers, or with dampers tuned to 250 Hz or 500 Hz, is still low, less than 2 dB/m, even though the

band is a stop band. The explanation may be that, at these frequencies, the pinned-pinned vibration of the rail, with either the fasteners behaving like pins, or the dampers behaving like pins, is still excited to some extent.

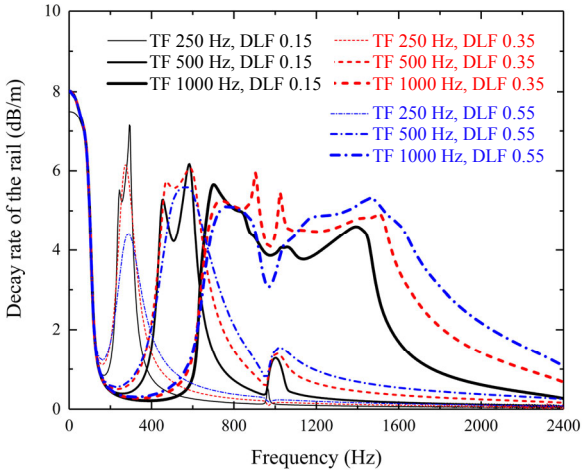

Fig. 13 Vibration decay rate of the rail

4.5 Vibration decay rates of the rail due to a moving harmonic load

For a moving harmonic load, the vibrations of the rail ahead of the load and behind the load are different, resulting in different vibration decay rates. Fig. 14 shows the ahead-load decay rates of the rail with dampers tuned to 250 Hz (thin lines), 500 Hz (thicker lines), and 1000 Hz (the thickest lines), and for the three values of damper loss factor: 0.15 (solid line), 0.35 (dashed line), and 0.55 (dash-dotted line). The load speed is 300 km/h, or 83 m/s.

It can be seen from Fig. 14 that the load speed may increase or decrease the decay rate, depending on the excitation frequency. For most of the frequencies, a higher damper loss factor results in a higher decay rate.

An observation may be made by comparing Fig. 13 and Fig. 14. For dampers tuned to 500 Hz, the small peak in Fig. 13 at a frequency slightly higher than 1000 Hz is not only enhanced by the load speed, but also shifted to a frequency lower than 1000 Hz, as shown in Fig. 14. Frequency shift is a normal phenomenon in moving load problems.

To see the effect of the load speed more clearly, the ahead-load and behind-load vibration decay rates of the rail are shown in Figs. 15–17 for the three damper frequencies. The damper loss factor is 0.35. For comparison, decay rates due to a stationary load are also shown by a solid line.

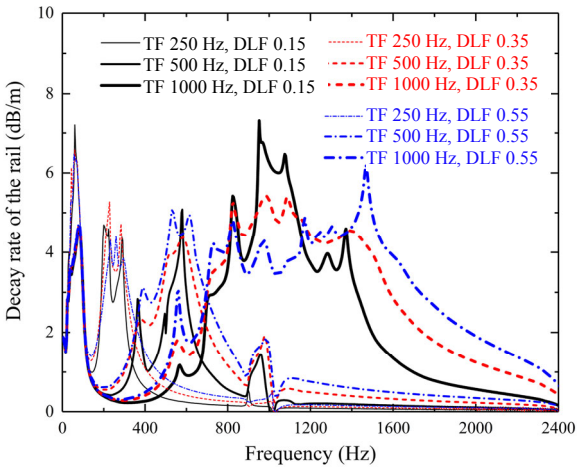

Fig. 14 Ahead-load decay rate of the rail

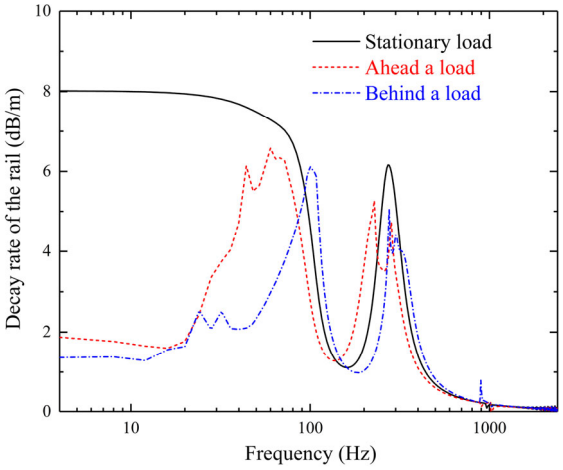

Fig. 15 Vibration decay rate (TF 250 Hz, DLF 0.35)

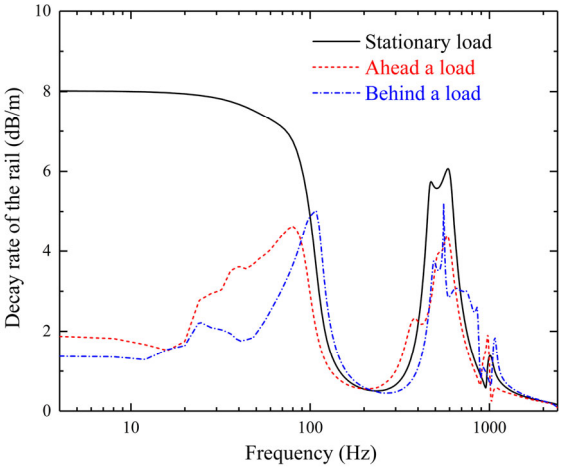

Fig. 16 Vibration decay rate (TF 500 Hz, DLF 0.35)

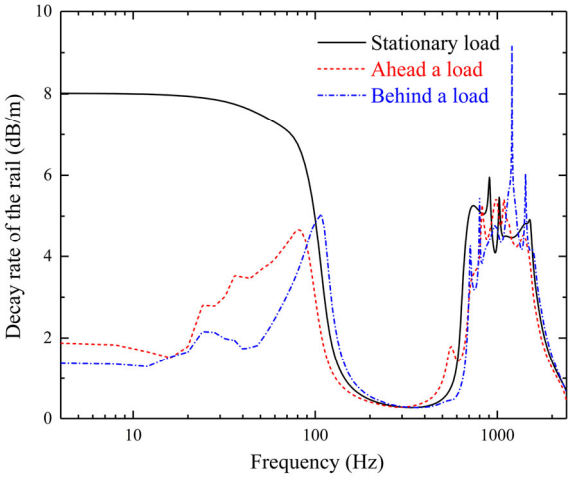

Fig. 17 Vibration decay rate (TF 1000 Hz, DLF 0.35)

It is seen from these figures that, in general, the load speed reduces the decay rate of the rail to some extent. This is partly because, even though the frequency of the load is within a stop band, a propagating wave may still be excited by the moving load. It is especially noticeable that, at frequencies lower than the first bounding frequency, the decay rate of the rail is significantly reduced by the load speed, and the reduction is greater for the behind-load decay rate than that for the ahead-load decay rate. However, when the damper is tuned to 1000 Hz, the ahead-load decay rate and the behind-load decay rate are similar to each other for load frequencies higher than 200 Hz.

4.6 Comparison in vibration energy level between different tracks due to a moving harmonic load

The main purpose of installing rail dampers is to reduce noise from the track, and at the same time not to significantly increase the wheel/rail force, ensuring a reduction in total rolling noise. Although installation of rail dampers can increase the decay rate of the rail vibration, it introduces extra radiators (the rail dampers). Thus, it may be asked if it is possible for the rail dampers to increase noise radiation from the track and wheel. To answer this question completely, an appropriate predictive model for noise radiation from the rail, dampers, and wheel is required. This model, however, is unavailable at the moment to the authors.

In this study, the vibration 'energy level' of a given length of a track is used to approximately indicate the potential for noise radiation of the track. For the original track, the vibration energy level is defined as

$$E = 10\lg\int_{-20L}^{20L} |\dot{w}(x', 0)|^2 \, \mathrm{d}x', \tag{19}$$

where $|\dot{w}(x', 0)|$ denotes the vertical velocity amplitude of the rail at x' and at the moment t=0. It can be seen in Eq. (19) that the given length of the track is 20 sleeper bays, or 13 m, either sides of the load. The length is chosen based on the fact that a point around 10 m away from the rail is often selected for noise measurement. For the track with rail dampers, the vibration energy level is defined to be

$$E = 10\lg\left[\int_{-20L}^{20L} |\dot{w}(x', 0)|^2 \, \mathrm{d}x' + L\sum_{j=-20}^{20} |\dot{w}_{\mathrm{D}j}(0)|^2\right], \tag{20}$$

where $|\dot{w}_{\mathrm{D}j}(0)|$ denotes the vertical velocity amplitude of the jth damper at the moment t=0. The numbers of dampers either sides of the load should be the same.

For the vibration energy level of the track to be a valid indicator of the noise performance of the dampers, the wheel/rail force must not be significantly altered by the rail dampers. To work out the frequency range within which this is true, Fig. 18 shows a comparison between the vertical displacement of the rail with dampers and a high-speed train wheel at the wheel/rail contact point due to a unit harmonic wheel/rail force moving at 83 m/s. The result for the wheel is taken from Sheng *et al.* (2016b), where the effect of the wheel rotation is included.

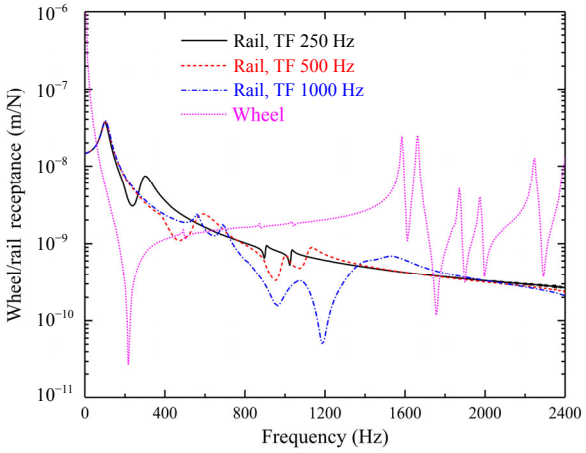

Fig. 18 Rail and wheel displacements

It can be seen from Fig. 18 that, for most of the frequencies higher than about 700 Hz, the displacement of the wheel is much higher than that of the rail. Thus, for these frequencies, the wheel/rail force is more controlled by the dynamics of the wheel than by the rail. In other words, for a given wheel/rail roughness, the wheel/rail force does not change significantly with rail dampers.

Fig. 19, for damper loss factor 0.15, shows vibration energy levels of the original track (solid line), the track with dampers tuned to 250 Hz (dashed line), the track with dampers tuned to 500 Hz (dash-dotted line), and the track with dampers tuned to 1000 Hz (dotted line). For another two values of damper loss factor, the results are shown in Figs. 20 and 21. The unit harmonic load is moving at 83 m/s, and at t=0 it is applied to the rail just above the 0th damper. It is noticed that oscillations appear in the curves for the original trace. Their cause has yet to be investigated.

It can be seen from these figures that: (1) for frequencies higher than about 700 Hz, all the damper designs can reduce the track vibration energy level to some extent, and dampers tuned to 1000 Hz are much better than the other two damper designs; (2) damping is beneficial in reducing the vibration energy level, however, its effect is not as strong as the tuned frequency; (3) to be effective, dampers tuned to a frequency much lower than the pinned-pinned frequency of the original track must have a high damping.

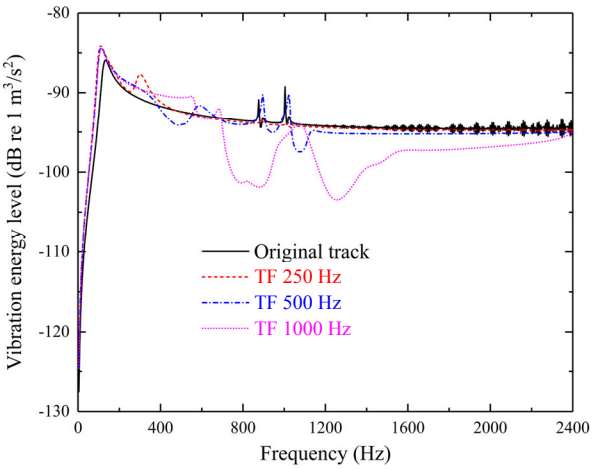

Fig. 19 Vibration energy level of the track (DLF 0.15)

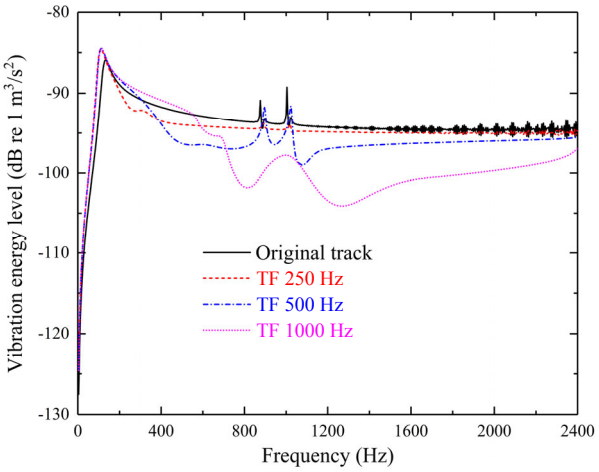

Fig. 20 Vibration energy level of the track (DLF 0.35)

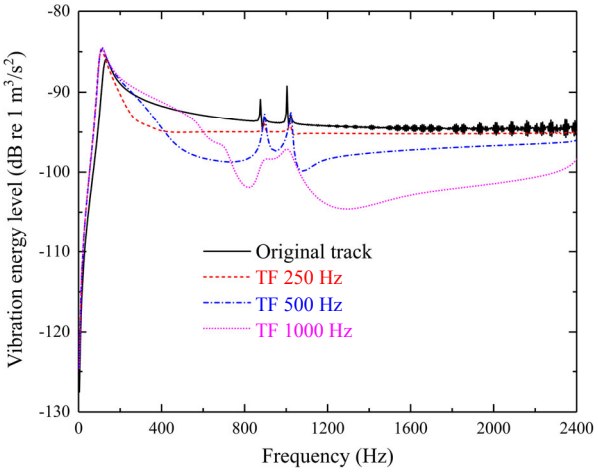

Fig. 21 Vibration energy level of the track (DLF 0.55)

4.7 Effect of damper mass

From Eq. (7) it can be seen that, at the tuned frequency, the receptance of the damper reaches a minimum, and this minimum decreases as the damper mass and/or stiffness increases, giving stronger restraint to the rail. The effect of the damper mass is investigated quantitatively in this section by fixing the tuned frequency at 1000 Hz. Thus, a change in mass implies a change in the stiffness by the same ratio (and the mass and stiffness for rotational vibration of the dampers also change by the same ratio). Fig. 22 shows the dispersion curves of the track with rail dampers tuned to 1000 Hz, but the mass and stiffness are halved. In the frequency range of 0 to 1500 Hz, the total width of the stop bands is 636 Hz. Fig. 23 shows the dispersion curves of the track with rail dampers tuned to 1000 Hz, but both the mass and

stiffness are doubled. In the frequency range of 0 to 1500 Hz, the total width of the stop bands is 900 Hz. Recall that with the original damper mass and stiffness, the total width of the stop bands is 809 Hz.

The vibration decay rate and vibration energy level are shown in Figs. 24 and 25.

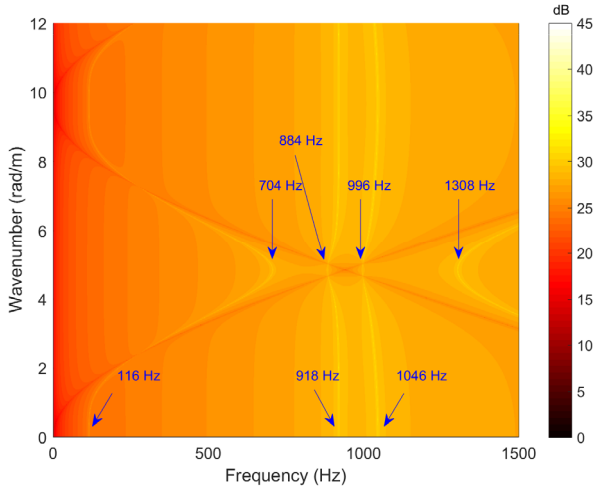

Fig. 22 Dispersion curves of the track with dampers tuned to 1000 Hz but with the mass and stiffness halved (bounding frequencies are 116, 704, 884, 918, 996, 1046, and 1308 Hz)

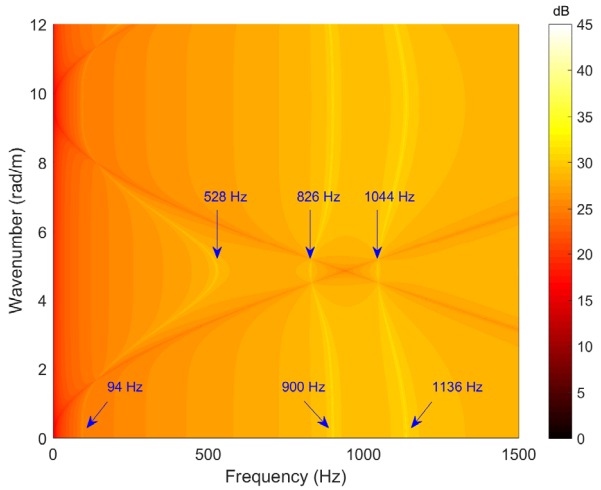

Fig. 23 Dispersion curves of the track with dampers tuned to 1000 Hz but with the mass and stiffness doubled (bounding frequencies are 94, 528, 826, 900, 1044, and 1136 Hz)

From Fig. 24, the frequency range in which the decay rate is higher than a given value is enlarged by increasing the damper mass and stiffness, and this enlargement is mainly achieved from the high frequency side. On the other hand, as shown in Fig. 25, there is still no effect on vibration energy level reduction for low frequencies even when damper mass and stiffness are doubled. The vibration energy gets worse when a damper with low mass is added, yet the decay rate is not evidently altered in this frequency region (Fig. 24). This is caused by the vibration energy in the dampers.

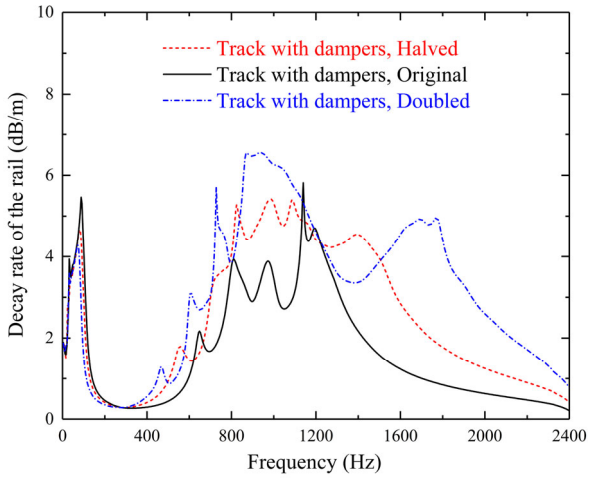

Fig. 24 Vibration decay of the rail with dampers

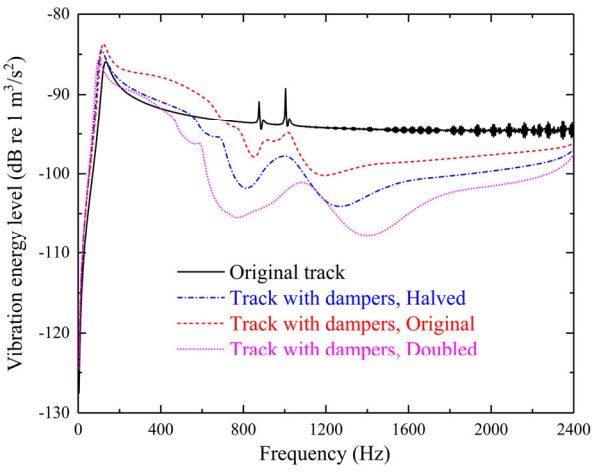

Fig. 25 Vibration energy level of the track

5 Conclusions

In this paper, a parametric study is performed to investigate the effect of rail dampers on the dynamical behavior of a Chinese high-speed railway track. The

Fourier transform-based method developed for analyzing dynamics of a railway track as an infinitely long periodic structure, with or without rail dampers, is applied for the investigation. Studied parameters include the tuned frequency, loss factor, and mass and stiffness of the dampers. Investigated dynamical behaviors of the track include: (1) dispersion curves of the track as an infinitely long periodic structure, showing stop bands, pass bands, and bounding frequencies; (2) receptance of the rail at the loading point and that of the damper just under the load, showing resonance characteristics of the track; (3) vibration decay rates of the rail and dampers due to a stationary harmonic load and a harmonic load moving at 300 km/h; (4) vibration energy level of the track with dampers indicating noise radiation potentials.

Physically, installation of rail dampers does not change the period of the track, but adds mass to the track and also creates constraints to the rail at midspans. Dynamically, installation of rail dampers introduces new bounding frequencies and stop bands, increasing the total width of stop bands and the vibration decay rate.

For a given load frequency, the rail vibration decay rate is different between a stationary load and a load moving at high speed, and in general, the decay rate for a moving load is lower than that for a stationary load. This is particularly true for load frequencies less than the first bounding frequency of the original track.

In terms of the total width of stop bands, the vibration decay rates of the rail and dampers, and the vibration energy level of the track, the damper should be tuned to a frequency close to the pinned-pinned frequency of the original track, and the mass and stiffness of the damper should be as high as possible. For the track considered in this paper, dampers tuned to other lower frequencies (but not too low compared to the pinned-pinned frequency) are also possible, if a high loss factor can be ensured for the dampers.

References

Correa, N., Vadillo, E.G., Santamaria, J., *et al*., 2012. A rational fraction polynomials model to study vertical dynamic wheel-rail interaction. *Journal of Sound and Vibration*, **331**(8):1844-1858. http://dx.doi.org/10.1016/j.jsv.2011.12.012

Croft, B.E., Jones, C.J.C., Thompson, D.J., 2009. Modelling the effect of rail dampers on wheel-rail interaction forces and roughness growth rates. *Journal of Sound and Vibration*, **323**(1-2):17-32. http://dx.doi.org/10.1016/j.jsv.2008.12.013

Han, J., Zhao, G.T., Xiao, X.B., *et al*., 2015. Effect of softening of cement asphalt mortar on vehicle operation safety and track dynamics. *Journal of Zhejiang University-SCIENCE A (Applied Physics & Engineering)*, **16**(12):976-986. http://dx.doi.org/10.1631/jzus.A1500080

Jin, X.S., 2014. Key problems faced in high-speed train operation. *Journal of Zhejiang University-SCIENCE A (Applied Physics & Engineering)*, **15**(12):936-945. http://dx.doi.org/10.1631/jzus.A1400338

Liu, H.P., Wu, T.X., Li, Z.G., 2009. Theoretical modelling and effectiveness study of rail vibration absorber for noise control. *Journal of Sound and Vibration*, **323**(3-5):594-608. http://dx.doi.org/10.1016/j.jsv.2009.01.036

Maes, J., Sol, H., 2003. A double tuned rail damper—increased damping at the two first pinned-pinned frequencies. *Journal of Sound and Vibration*, **267**(3):721-737. http://dx.doi.org/10.1016/S0022-460X(03)00736-3

Mazilu, T., 2007. Green's functions for analysis of dynamic response of wheel/rail to vertical excitation. *Journal of Sound and Vibration*, **306**(1-2):31-58. http://dx.doi.org/10.1016/j.jsv.2007.05.037

Mazilu, T., Dumitriu, M., Tudorache, C., *et al*., 2011. Using the Green's functions method to study wheelset/ballasted track vertical interaction. *Mathematical and Computer Modelling*, **54**(1-2):261-279. http://dx.doi.org/10.1016/j.mcm.2011.02.009

Mead, D.J., 1996. Wave propagation in continuous periodic structures: research contributions from Southampton. *Journal of Sound and Vibration*, **190**(3):495-524. http://dx.doi.org/10.1006/jsvi.1996.0076

Nordborg, A., 2002. Wheel-rail noise generation due to nonlinear effects and parametric excitation. *The Journal of the Acoustical Society of America*, **111**(4):1772-1781. http://dx.doi.org/10.1121/1.1459463

Sheng, X., 2015. Generalization of the Fourier transform-based method for calculating the response of a periodic railway track subject to a moving harmonic load. *Journal of Modern Transportation*, **23**(1):12-29. http://dx.doi.org/10.1007/s40534-015-0066-2

Sheng, X., Li, M., 2007. Propagation constants of railway tracks as a periodic structure. *Journal of Sound and Vibration*, **299**(4-5):1114-1123. http://dx.doi.org/10.1016/j.jsv.2006.08.010

Sheng, X., Xiao, X., 2015. Calculation of moving Green functions for high-speed railway tracks. Proceedings of the 24th Symposium of the International Association for Vehicle System Dynamics, p.1355-1366. http://dx.doi.org/10.1201/b21185-144

Sheng, X., Jones, C.J.C., Thompson, D.J., 2005. Responses of infinite periodic structures to moving or stationary harmonic loads. *Journal of Sound and Vibration*, **282**(1-2): 125-149. http://dx.doi.org/10.1016/j.jsv.2004.02.050

Sheng, X., Liu, Y., Zhou, X., 2016a. The response of a high-speed train wheel to a harmonic wheel-rail force. *Journal of Physics: Conference Series*, **744**(1):012145. http://dx.doi.org/10.1088/1742-6596/744/1/012145

Sheng, X., Xiao, X., Zhang, S., 2016b. The time domain moving Green function of a railway track and its application to wheel-rail interactions. *Journal of Sound and Vibration*, **377**:133-154. http://dx.doi.org/10.1016/j.jsv.2016.05.011

Thompson, D.J., 2008. A continuous damped vibration absorber to reduce broad-band wave propagation in beams. *Journal of Sound and Vibration*, **311**(3-5):824-842. http://dx.doi.org/10.1016/j.jsv.2007.09.038

Thompson, D.J., 2009. Railway Noise and Vibration: Mechanisms, Modelling and Means of Control. Elsevier, Oxford, UK, p.221-279.

Thompson, D.J., Jones, C.J.C., Waters, T.P., *et al*., 2007. A tuned damping device for reducing noise from railway tracks. *Applied Acoustics*, **68**(1):43-57. http://dx.doi.org/10.1016/j.apacoust.2006.05.001

Wu, T.X., 2008. On the railway track dynamics with rail vibration absorber for noise reduction. *Journal of Sound and Vibration*, **309**(3-5):739-755. http://dx.doi.org/10.1016/j.jsv.2007.07.049

Zhai, W., Wei, K., Song, X., *et al*., 2015. Experimental investigation into ground vibrations induced by very high speed trains on a non-ballasted track. *Soil Dynamics and Earthquake Engineering*, **72**:24-36. http://dx.doi.org/10.1016/j.soildyn.2015.02.002

中文概要

题　目： 钢轨减振器对高铁轨道结构动力学特性的影响研究

目　的： 针对典型高铁轨道结构，对钢轨减振器的设计参数进行研究，进一步揭示钢轨减振器的工作机理，为合理设计和应用提供科学依据。

创新点： 运用基于傅里叶变换的无限长周期结构动态特性的分析方法，从轨道结构的频散特性、共振特性、振动衰减特性和振动能量（近似声辐射能力）等多个方面对钢轨减振器的参数进行研究；提出荷载移动对振动衰减率的影响问题。

方　法： 运用基于傅里叶变换的无限长周期结构动态特性的分析方法，结合典型高铁轨道结构，对钢轨减振器的设计参数对轨道结构动力学特性的影响进行研究。研究的动力学特性包括：频散特性、共振特性、振动衰减特性和振动能量（近似声辐射能力）。

结　论： 1. 加装钢轨减振器会引入新的阻带，从而增加整个阻带的宽度；2. 在移动和不移动的情况下，荷载的振动衰减率是不同的；荷载的高速移动会降低振动衰减率；3. 从阻带尽量宽、振动衰减率尽量大和振动能量尽量小这三方面的要求来看，钢轨减振器的设计频率应该接近原来轨道结构的 Pinned-Pinned 频率，并且质量越大越好；4. 如果能够保证足够高的阻尼，钢轨减振器的频率可以设计得比 Pinned-Pinned 频率低。

关键词： 钢轨减振器；轨道动力学；频散曲线；振动衰减率